Investigation of the carbonation front shape on cementitious materials: Effects of the chemical kinetics

M. Thiery [*], G. Villain [1], P. Dangla [1], G. Platret [1]

Laboratoire Central des Ponts et Chaussées, 58 boulevard Lefèbvre — 75015 — Paris, France

Abstract

Carbonation depth-profiles have been determined by thermogravimetric analysis and by gammadensitometry after accelerated carbonation tests on ordinary Portland cement (OPC) pastes and concretes. These methods support the idea that carbonation does not exhibit a sharp reaction front. From analytical modelling, this feature is explained by the fact that the kinetics of the chemical reactions become the rate-controlling processes, rather than the diffusion of CO_2. Furthermore, conclusions are drawn as to the mechanism by which carbonation of $Ca(OH)_2$ and C–S–H takes place. Carbonation gives rise to almost complete disappearance of C–S–H gel, while $Ca(OH)_2$ remains in appreciable amount. This may be associated with the $CaCO_3$ precipitation, forming a dense coating around partially reacted $Ca(OH)_2$ crystals. The way in which CO_2 is fixed in carbonated samples is studied. The results indicate that CO_2 is chemically bound as $CaCO_3$, which precipitates in various forms, namely: stable, metastable, and amorphous. It seems that the thermal stability of the produced $CaCO_3$ is lower when the carbonation level is high. It is also shown that the poorly crystallized and thermally unstable forms of $CaCO_3$ are preferentially associated with C–S–H carbonation.
© 2007 Elsevier Ltd. All rights reserved.

Keywords: Kinetics (A); Thermal analysis (B); Carbonation (C); $CaCO_3$ (D); $Ca(OH)_2$ (D)

1. Introduction

Reinforcing bars in concrete are protected from corrosion by a thin oxide and hydroxide layer, which is formed on the steel surface because of the high pH-value (pH $\geq$ 13) of the surrounding concrete. Corrosion may start when this protective layer is destroyed by a decrease of the pH-value. Such a reduction in alkalinity can be the result of $Ca(OH)_2$ carbonation in the concrete mass. The physicochemical processes [1] involved in $Ca(OH)_2$ carbonation are: the diffusion of CO_2 in the gaseous phase of the concrete pores, the dissolution of CO_2 in the pore water as carbonic acid H_2CO_3, its dissociation as HCO_3^- and CO_3^{2-} ions, the dissolution of solid $Ca(OH)_2$, releasing calcium Ca^{2+} and hydroxyl OH^- ions, and the precipitation of Ca^{2+} with CO_3^{2-} forming $CaCO_3$. These intermediate reactions are synthesized in the following overall chemical reaction:

$$Ca(OH)_2 + CO_2 \rightarrow CaCO_3 + H_2O \qquad (1)$$

Eq. (1) indicates that $Ca(OH)_2$ carbonation sets free water that was initially combined in $Ca(OH)_2$. This supply of water was experimentally highlighted by Pihlajavaara [2].

It is well-known that not only $Ca(OH)_2$, but also all the other hydrated compounds can react with CO_2. The reaction between CO_2 and the calcium silicate hydrates (C–S–H) produces $CaCO_3$ and a silica gel [3–6]. Ettringite (trisulfate hydrates AFt) and monosulfate hydrates (AFm) are abundant when certain cements are used, especially in the case of a rapid-hardening cement with a high C_3A content, or a cement mixed with a large amount of gypsum. It has been established [7–9] that AFt decomposes by carbonation to $CaCO_3$, gypsum and alumina gel.

Because the carbonation products have higher molar volumes than the parent hydrates $Ca(OH)_2$ and C–S–H, a decrease of porosity is expected. The materials made of ordinary Portland cement (OPC) actually show a pronounced reduction in pore

* Corresponding author. Tel.: +33 1 40 43 52 41; fax: +33 1 40 43 54 98.
  E-mail address: thiery@lcpc.fr (M. Thiery).
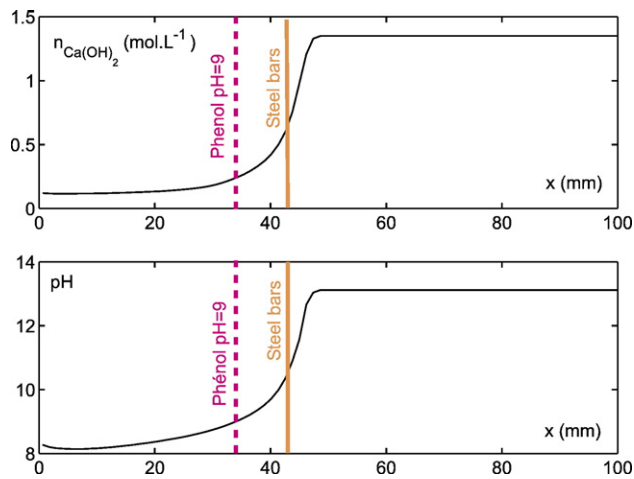[1] Tel.: +33 1 40 43 52 41; fax: +33 1 40 43 54 98.

Fig. 1. Schematic sketches of $Ca(OH)_2$ content and pH-profiles in the concrete cover when the concrete has been carbonated to a certain depth.

Table 2
Mix compositions and main characteristics of studied concrete mixtures

Reference	B25	B40	B50
Gravel (G) (kg/m^3)	1007	1001	937
(min/max grain size in mm)	5/12.5	5/12.5	5/12.5
Sand (S) (kg/m^3)	899	897	806
(min/max grain size in mm)	0/5	0/5	0/5
Cement (C) (kg/m^3)	230	300	410
Water (W) (kg/m^3)	193	187	197
Water-to-cement ratio (W/C)	0.84	0.62	0.48
28-day compressive strength (MPa)	24.0±3.6	41.0±1.0	54.8±1.0
90-day porosity accessible to water (%)	14.8±0.5	14.4±0.4	13.6±0.3
90-day $Ca(OH)_2$ content (mol/L)	1.3±0.1	1.2±0.1	1.8±0.2

because steel corrosion can be observed at a pH-value higher than 9 [20]. Since the phenolphthalein measurement does not show the changes which may occur in partially carbonated concrete, the use of carbonation depth-profiles is required.

The paper uses two methods to evaluate carbonation depth-profiles: the thermogravimetric technique and the gammadensitometry. They are applied on a cement paste and three concrete mixes (with the same OPC), exposed to accelerated carbonation. The comparison of the results contributes to the understanding of the kinetics of $Ca(OH)_2$ and C–S–H carbonation, and makes it possible to study the thermal stability of precipitated $CaCO_3$. Furthermore, a theoretical study is proposed to understand the fact that the carbonation front is gradual and to link it to the kinetics of the chemical reactions which are at stake. In the light of an analytical model, it is established that these kinetics become rate-controlling processes, rather than the diffusion of CO_2, and may account for the existence of a partially carbonated area.

2. Experimental procedure

2.1. Materials

The cement used is an ordinary Portland cement OPC, whose chemical composition and mineral composition by Bogue's formula are given in Table 1. The cement has a low C_3A content so AFt and AFm are minor components. When the cement is hydrated, $Ca(OH)_2$ and C–S–H hydrates comprise in this case most of the carbonatable cementitious matrix.

A cement paste (P45, W/C=0.45) was prepared: cylindrical moulds (ϕ=3.2 cm and h=8 cm) of the fresh cement paste were rotated for 24 h to avoid any sedimentation. The moulds were removed after 24 h, and the specimens were wrapped in two sheets of adhesive aluminium foil. They were stored at a temperature of 20 °C and a relative humidity RH of 95%±5%

volume due to carbonation. This feature is based on the examination of water sorption isotherms [2] before and after carbonation, on mercury intrusion porosimetry measurements [2,10–12], and on gammadensitometry results [12]. Nevertheless, concrete made with Portland cement shows a different behaviour than materials made with cement blended with mineral admixtures (e.g., blast furnace slag, fly ashes, or silica fumes) whose carbonation can cause a higher porosity, and thus a lowering of the durability [13].

Moisture is an essential parameter for carbonation reaction to occur. A low environmental relative humidity RH induces drying of the capillary pores, which slows down the dissolution–dissociation of CO_2, and the dissolution of hydrates. On the other hand, a high environmental RH delays the CO_2 diffusion into concrete, because of capillary water condensation in the pores. For optimum carbonation, the environmental RH should be varying between 50% and 70% [14,15].

Using the phenolphthalein indicator solution to monitor the carbonation depth has been well documented. The solution is a colourless acid/base indicator, which turns purple when the pH-value is above 9. However, this test does not indicate the depth of maximum ingress of CO_2. Actually, the penetrating gas can have reacted at greater depths of the concrete, causing a decrease in the pH-value beyond the carbonation depth indicated by the phenolphtalein spray test, as illustrated in Fig. 1. $CaCO_3$ formation beyond the phenolphthalein-purple border has been demonstrated by means of thermoanalytical methods [12,16–18,28], and by means of infrared spectroscopy [19]. The observed partial carbonation does not develop without danger,

Table 1
Chemical and mineral composition (calculated by Bogue's formula) of the OPC cement used (all values are in mass %)

LOI	Insol.	CaO	SiO$_2$	Fe$_2$O$_3$	Al$_2$O$_3$	TiO$_2$	MgO	Na$_2$O	K$_2$O	MnO	SO$_3$
1.2	0.8	65.4	20.5	4.1	3.6	0.2	0.9	0.2	0.3	0.1	2.7

C$_3$S	C$_2$S	C$_4$AF	C$_3$A	CaCO$_3$	Gypsum	Free CaO
57.6	17.8	12.6	2.2	2.0	6.15	0.7

Insol.: insoluble residue. LOI: loss on ignition.

during 8 months prior to carbonation exposure. After such a curing, the porosity accessible to water (measured by hydrostatic weighing) was equal to $40.0\pm1.6\%$, and the initial $Ca(OH)_2$ content, measured by thermogravimetric analysis, was estimated around 5.8 ± 0.5 mol L^{-1}.

Three concrete mixes were studied (B25, B40 and B50) whose main characteristics are summarized in Table 2. The specimens were cast inside $\phi=11$ cm/$h=22$ cm cardboard moulds which were stripped after 24 h, and then placed under water at 20 °C for 90 days (water-curing).

2.2. Pre-treatment of the specimens

After the end of the 90-day wet curing period, slices ($\phi=11$ cm/$h=6$ or 10 cm) were sawn from the concrete specimens. They were all covered with two sheets of adhesive aluminium foil, with the exception of the two opposite lateral faces to ensure unidirectional drying and carbonation. Then, the concrete specimens were oven-dried at 45 °C during 1 month to facilitate the CO_2 diffusion through a larger pore network which is freed of capillary water.

After curing, the cement paste P45 specimens were sawn in half, leaving a side face exposed to drying and carbonation. The program continued with a 1-month drying at 45 °C and an 8-month storage in sealed cells, in which RH is controlled at 53% and $T=20$ °C.

2.3. Experimental program of accelerated carbonation

Because in normal environments (which contain 0.03% to 0.1% CO_2), the evolution of the carbonation depth with time is extremely slow, the carbonation test was done inside a chamber with a CO_2 concentration $\approx 50\%\pm5\%$, RH $\approx 53\%\pm5\%$, and $T\approx 21$ °C±1 °C. The imposed RH $\approx 53\%$ is chosen in such a way that the carbonation rate is maximum.

Tests were carried out at various exposure durations: 3, 7, 14 and 28 days. At each date, two concrete specimens ($\phi=11$ cm/$h=6$ cm) and two cement paste specimens ($\phi=3.2$ cm and $h=4$ cm) were split by half along a diameter. The fresh-split surfaces were sprayed with a 1% phenolphthalein pH-indicator to measure the average carbonation depth. Furthermore, at each stage, a concrete specimen ($\phi=11$ cm/$h=10$ cm) was analysed by gammadensitometry. After 14 days of accelerated exposure, one concrete cylinder was sawn into slices (about 4–5 mm in thickness), perpendicular to the CO_2-diffusion direction. Then, a piece of the mortar phase was extracted from each slice and crushed for the quantification of $Ca(OH)_2$ and $CaCO_3$ by a thermogravimetric analysis (TGA) coupled with a chemical analysis (CA) according to the method described in [18]. For the cement paste, the sawing was carried out (slices with about 1–2 mm thickness) after 14 and 28 days of accelerated carbonation.

2.4. Gammadensitometry and thermogravimetric analysis

Gammadensitometry makes it possible to characterise the concrete specimens by monitoring the evolution of their density according to depth and time. It is used to determine water profiles in specimens exposed to drying [21]. In this case, the
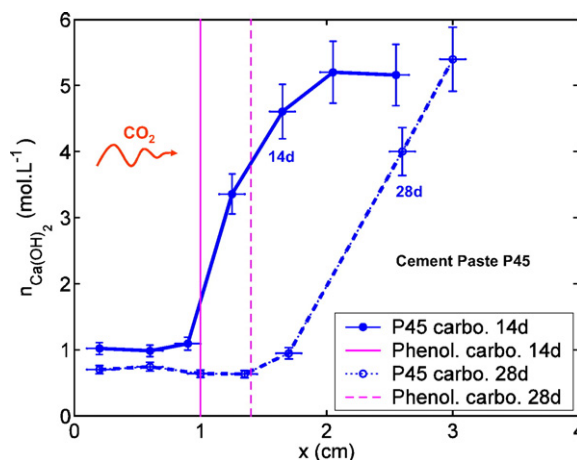

Fig. 2. $Ca(OH)_2$ depth-profiles after 14 days and 28 days of accelerated carbonation of the cement paste P45. Mean carbonation depths determined by the phenolphthalein spray-test.

local evolution of moisture content is related to the variation of mass density of the material. Gammadensitometry can also measure the local density increase due to carbonation [12,21,28]. By assuming that no significant water migration by drying occurs in the short run of 28 days of accelerated carbonation of the oven-dried concrete specimens, the measured density increase can be related solely to CO_2 fixation [21,28].

Thermogravimetric analysis TGA is used to assess the amount of precipitated $CaCO_3$, and also the amount of $Ca(OH)_2$ remaining in an uncarbonated form. In TGA, the weight changes are determined as the sample is heated at a uniform rate of 10 °C min^{-1} from 25 to 1150 °C in a gas flow of air. The first derivative of mass change (DTG) is used for identification purposes, as it yields sharp peaks. The mass loss around 430–520 °C corresponds to the $Ca(OH)_2$ dehydration (emission of H_2O). The determination of $CaCO_3$ formed after carbonation offers some difficulty, because of the relatively large temperature range (≈ 400 °C centred on approximately 750 °C) over which the weight loss due to the CO_2 dissociation occurs.

Since the mortar sample (≈ 200 mg), taken from each sawn slice by avoiding aggregate and analysed by TGA, is not representative of the overall mix design, it is necessary to determine its real cement content. The purpose is to express the $Ca(OH)_2$ (or $CaCO_3$) molar quantities for the same volume V_0 of material, independently of the carbonation and moisture states of the sawn slices, and also of the possible cement sedimentation and concrete heterogeneities due to the presence of aggregates. The volume V_0 is chosen to be a reference volume of water saturated and non-carbonated material. This cement content has to be determined by means of a chemical analysis (CA) which is carried out on each sample analysed by TGA, as shown in [18].

3. Experimental results

3.1. ATG and DTG results obtained on the carbonated cement paste

Fig. 2 shows typical $Ca(OH)_2$ profiles obtained by TGA for the cement paste P45 after 14 and 28 days of accelerated

exposure. The carbonation depths obtained by the phenolphthalein spray-test are also indicated. These data support the idea that $Ca(OH)_2$ carbonation does not exhibit a sharp reaction front, as already suggested by Parrott and Killoh [22] for *in situ* conditions, and by Rahman and Glasser for accelerated conditions [16].

The $Ca(OH)_2$ profiles and the position of the carbonation front determined by the pH-indicator spray-test suggest that $Ca(OH)_2$ carbonation develop three zones. The first (or inner zone) corresponds to uncarbonated material. Next, is an intermediate (or transitional) zone where the $Ca(OH)_2$ content progressively increases with distance from the surface. Finally, an outer zone is encountered, just in front of the phenolphtalein neutralization depth, where not all the $Ca(OH)_2$ is depleted. This remaining $Ca(OH)_2$ is not sufficiently accessible to maintain a pH-value above 9 in the pore solution.

This residual $Ca(OH)_2$ in the carbonated area could be explained by the formation of a $CaCO_3$ coating around the $Ca(OH)_2$ crystals, as has already been observed by Groves et al. [23,24] in transmission electron microscopy of carbonated hardened C_3S cement pastes. The accessibility of $Ca(OH)_2$ is thus reduced, since the diffusion rate of ions (such as Ca^{2+}, OH^- and CO_3^{2-}) is limited through the micro-porous and tortuous $CaCO_3$ coating. This phenomenon both hinders the $Ca(OH)_2$ dissolution, which is necessary to buffer the pH-value, and the precipitation of $CaCO_3$. It justifies that, after a period of rapid consumption, the $Ca(OH)_2$ carbonation rate is drastically reduced, as it was observed by Dunster [25]. This result can be corroborated with the chemical study of Glasson [26], who outlined that this $CaCO_3$ layer which develops around $Ca(OH)_2$ crystals becomes more compact at pH levels around 8–10, especially in the presence of HCO_3^- ions (i.e., for pH<10.3) which are present when the level of carbonation is sufficiently high.

Fig. 3 illustrates DTG diagrams of samples taken at different depths of the P45 cement paste after a 14-day accelerated carbonation test. The peak due to the dehydration of $Ca(OH)_2$ is
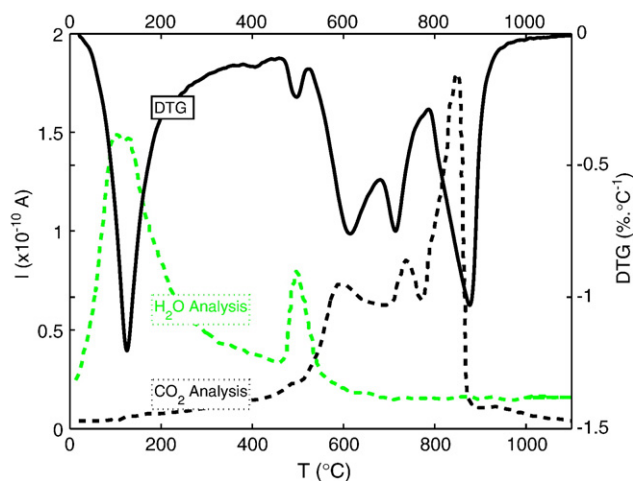
Fig. 4. DTG data and results of mass spectroscopy (ion currents for H_2O and CO_2) determined in a 2 mm-deep sample (T1) of the cement paste P45 after 14 days of accelerated carbonation.

logically reduced in intensity since the samples are taken close to the surface which is exposed to CO_2. A general trend is found for the influence of the level of carbonation on the temperature range of $CaCO_3$ decomposition: it seems that the higher the level of carbonation is, the more $CaCO_3$ seems to decompose at lower temperature, and thus to be thermally unstable. Three modes of decomposition can be distinguished, and progressively appear when the level of carbonation increases: first, mode I (780 °C<T<990 °C]), then, mode II (680 °C<T<780 °C), and finally, mode III (550 °C<T<680 °C). These three modes coexist in the ultimate state of carbonation. According to Sauman [3], mode I would be due to the decomposition of well-crystallized $CaCO_3$, namely calcite. By X-ray diffraction, Sauman also identified metastable phases of $CaCO_3$ (vaterite and aragonite) which are transformed into calcite when heated to 440–470 °C according to an allotropic transformation. Because of its less perfect crystalline state and high dispersity, the calcite produced is thermally less stable and preferentially decomposes within the temperature range of mode II. The thermal mode III is more difficult to explain. One wonders if it can be really attributed to a CO_2 emission. Several studies [3,27,28] reported the existence of a similar broad thermal effect in the same temperature range. Cole and Kroone [27] demonstrated that the CO_2 amount measured by TGA in the temperature range 650–950 °C (modes I and II) largely underestimates all the chemically fixed CO_2 which is measured in OPC carbonated specimens of mortar. Thus, they showed that only a small part of the CO_2 content is due to the $CaCO_3$ which is decomposed in the standard temperature ranges of modes I and II. To corroborate these data with our results, a mass spectrometer was coupled with the thermogravimetric analyser used in this study, in order to detect which gas (H_2O or CO_2) is emitted during the heating. The corresponding results are given in Fig. 4 for a sample taken close to the surface of the P45 cement paste, where the level of carbonation is the highest. This figure confirms that mode III is essentially linked to an emission of CO_2, like modes I and II.
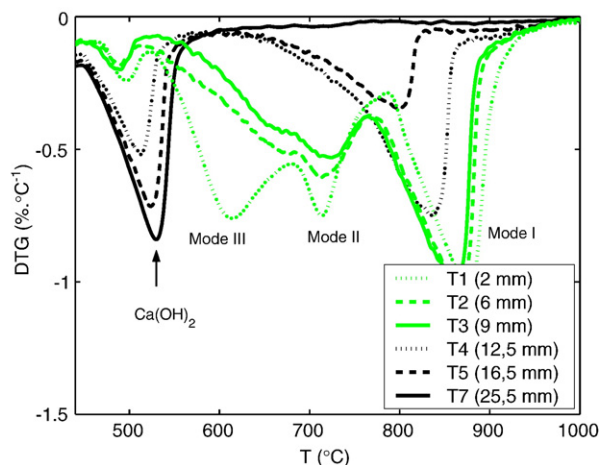
Fig. 3. DTG data obtained from samples extracted at different depths of the cement paste P45 after 14 days of accelerated carbonation. Zoom in the temperature range 450–1000 °C.
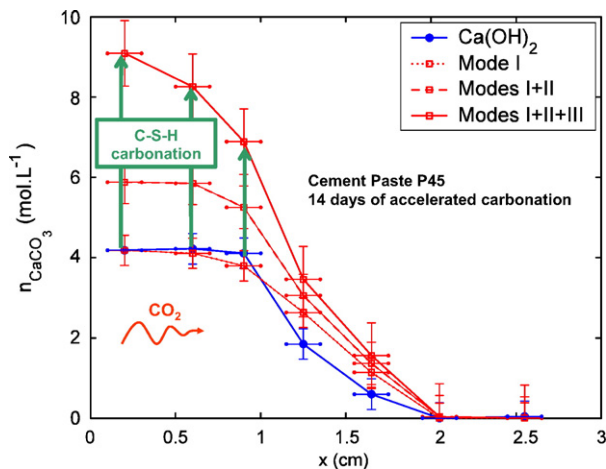
Fig. 5. CaCO$_3$ profiles for the cement paste P45 after 14 days of accelerated carbonation. Profiles corresponding to CaCO$_3$ produced by the sole carbonation of Ca(OH)$_2$ and to the three DTG modes of CaCO$_3$ decomposition.

Kondo et al. [29] studied the crystallinity of the various forms of CaCO$_3$ which are produced after carbonation. They demonstrated that the total amount of crystallized CaCO$_3$ (which can be determined by X-ray diffraction) underestimates the carbon dioxide which is quantified by a chemical analysis. This discrepancy is evidence that amorphous CaCO$_3$ is likely to form. It could also be explained by the presence of absorbed CO$_2$ or carbonates ions (such as CO$_3^{2-}$ or HCO$_3^-$). It should be emphasized that the polymorphism of CaCO$_3$ has been broadly studied by chemists. It has been shown that, CaCO$_3$ can precipitate from aqueous solution in various metastable forms [30–33]. Three anhydrous crystalline polymorphs are known: calcite, vaterite, and aragonite. They may correspond to thermal modes I and II. Calcite is the most stable form at ordinary temperatures and pressures. In addition, amorphous calcium carbonate has also been characterized previously [31]. It could be associated with the thermal mode III.

The use of a high concentration of CO$_2$ and a pre-treatment by oven-drying may of course influence the carbonation mechanism. For instance, the acceleration conditions favour the CaCO$_3$ precipitation just around the Ca(OH)$_2$ crystals. On one hand, the mobility of CO$_3^{2-}$ and Ca^{2+} ions is reduced because of a lack of water in the pores. On the other hand, the rates of the chemical reactions are so accelerated by a high CO$_2$ concentration that Ca^{2+} ions cannot migrate in the pore solution in the short term of the accelerated carbonation test to precipitate with CO$_3^{2-}$ ions far from the Ca(OH)$_2$ crystals surface. Moreover, the presence of metastable (vaterite and aragonite) and amorphous CaCO$_3$ in the carbonated area seems to be a feature of accelerated carbonation tests. Actually, these CaCO$_3$ forms are not stable in the temperature and pressure range under consideration, and in contact with water, they are transformed into calcite *via* dissolution–reprecipitation, as reported by Ogino et al. [30]. For that reason, they may persist for a long time in a dry environment. For our materials, which are oven-dried, the interstitial solution is just an aqueous film, and so, the conversion process of vaterite, aragonite and amorphous CaCO$_3$ is drastically reduced, and may not occur.

3.2. Carbonations profiles obtained on the carbonated cement paste

Fig. 5 shows TGA CaCO$_3$ profiles obtained for the P45 cement paste after a 14-day carbonation test. They are determined by considering the temperature ranges of the modes I, I+II, I+II+III. The CaCO$_3$ profile corresponding to the sole carbonation of Ca(OH)$_2$ is also added: it is calculated by subtracting the residual content at a certain depth from the initial Ca(OH)$_2$ amount estimated in the non-carbonated area. The results make it clear that Ca(OH)$_2$ carbonation preferentially corresponds to the precipitation of thermally stable CaCO$_3$ which is associated with mode I, and which represents well crystallized calcite. A proof that compounds, other than Ca(OH)$_2$, can also be carbonated (essentially C–S–H) is that the total amount of CaCO$_3$ produced (modes I+II+III) exceeds that which would correspond solely to the Ca(OH)$_2$ carbonation. Since the temperature ranges of the three modes I, II and III overlap, it is difficult to carry out a rigorous separation of them. However, the profile corresponding to the three modes I+II+III is relatively reliable, given that it expresses the total CaCO$_3$ amount which is present in the sample, and does not require any distinction of the temperature ranges. From these observations, it is deduced that the CaCO$_3$ amount which is produced by the C–S–H carbonation can be calculated starting from the difference between the CaCO$_3$ profile associated with Ca(OH)$_2$ carbonation and that which is related to the total CaCO$_3$ amount (modes I+II+III), as it is illustrated in Fig. 5.

Fig. 6 illustrates Ca(OH)$_2$ and C–S–H carbonation profiles after a 14-day and a 28-day accelerated carbonation test of the P45 cement paste.

In Fig. 6, the maximum contents of CaCO$_3$ which can precipitate after Ca(OH)$_2$ or C–S–H carbonation are calculated:

– for Ca(OH)$_2$ thanks to the TGA measurement of the initial Ca(OH)$_2$ content in the cement paste;
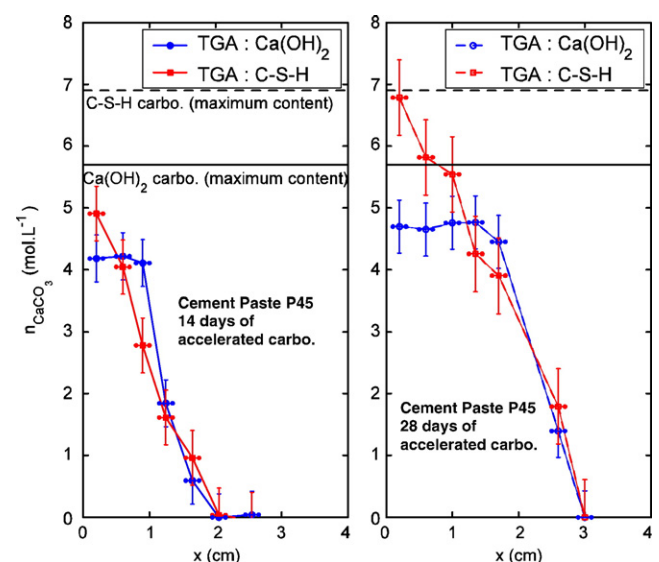

Fig. 6. Ca(OH)$_2$ and C–S–H carbonation profiles after a 14-day and a 28-day accelerated carbonation test of the cement paste P45.

– for C–S–H by making the assumptions that C_3S and C_2S phases are completely hydrated, that the C–S–H stoichiometry is $C_{1.7}SH_z$, and that each mole of C–S–H produces after carbonation 1.7 moles of $CaCO_3$.

The $Ca(OH)_2$ and C–S–H carbonation profiles are gradual. It seems that the carbonation of these two hydrates can be simultaneous, after a first period during which $Ca(OH)_2$ carbonation appears to have priority. During the carbonation process, $Ca(OH)_2$ consumption slows down and the reaction is progressively stabilized when the level of carbonation is sufficiently high (e.g. ≈70% after 14 days of accelerated exposure), whereas the C–S–H gel reacts continuously, at relatively constant rate, until reaching a maximum level on the surface of the specimen after a 28-day carbonation test. These observations are in agreement with those of Hunt and Tomes [34], which indicate that C–S–H may carbonate while the $Ca(OH)_2$ consumption is blocked. An explanation of this phenomenon is that C–S–H hydrates offer a greater reactive surface than coarser $Ca(OH)_2$ crystals. Consequently, the formation of a dense impermeable $CaCO_3$ layer does not reduce the accessibility in a way as pronounced as for massive $Ca(OH)_2$ crystals. Therefore, it appears that thermodynamic considerations, which make it possible to show that the C–S–H carbonation follows $Ca(OH)_2$ carbonation [35], remain insufficient to describe the carbonation process.

3.3. Carbonation profiles in carbonated concrete specimens

Fig. 7 shows CO_2 content profiles measured by gammadensitometry and by TGA on the three studied concretes after a 14-day accelerated carbonation test. Gammadensitometry can detect all forms of CO_2 in the carbonated material: in the

gaseous phase, in aqueous solution as H_2CO_3, HCO_3^- and CO_3^{2-}, as absorbed CO_2 in the C–S–H gel, and as chemically bound in $CaCO_3$. It is possible to calculate the maximum concentrations of free CO_2 at equilibrium in the gaseous and aqueous phases for the chemical system $CaCO_3$–$Ca(OH)_2$–CO_2–H_2O. Up to a partial CO_2–pressure of 5000 kPa (50% CO_2–50% air) at 20 °C, these concentrations are very small. For instance, the molar contents of free CO_2 are lower than the following values: $\phi(1-S)[CO_2] \leq 0.003$ mol L^{-1} in the gaseous phase, and $\phi S([H_2CO_3]+[HCO_3^-]+[CO_3^{2-}]) \leq 0.0045$ mol L^{-1} in aqueous solution, by assuming a porosity $\phi=0.15$ and a saturation degree respectively $S=0$ and $S=1$. Consequently, the experimental assessment of the CO_2 content by gammadensitometry has an uncertainty (i.e. 0.07 mol L^{-1} [28]) that largely exceeds these maximum CO_2 contents in the aqueous and gaseous phases. Furthermore, from the agreement between TGA and gammadensitometry, as shown in Fig. 7, it may be deduced that the absorbed ratio of total fixed CO_2 in the concrete is negligible, compared with the carbon dioxide chemically bound as $CaCO_3$ which TGA detects.

3.4. Influence of the water content on the kinetic of carbonation

Prior to exposure to carbonation, the concrete specimen were oven-dried at 45 °C during 1 month (pre-treatment S1). A stronger pre-treatment was also tested (pre-treatment S2): 1 week at 45 °C, 2 weeks at 60 °C and 1 week at 45 °C. Fig. 8a represents the depth-profiles of saturation degree which are obtained by gammadensitometry for concrete B40 at the end of the two pre-treatments S1 and S2. Fig. 8b illustrates the corresponding gammadensimetric CO_2 profiles content after a 14-day carbonation test. It seems that carbonation penetrates the concrete more deeply because it is dry, and because space is left
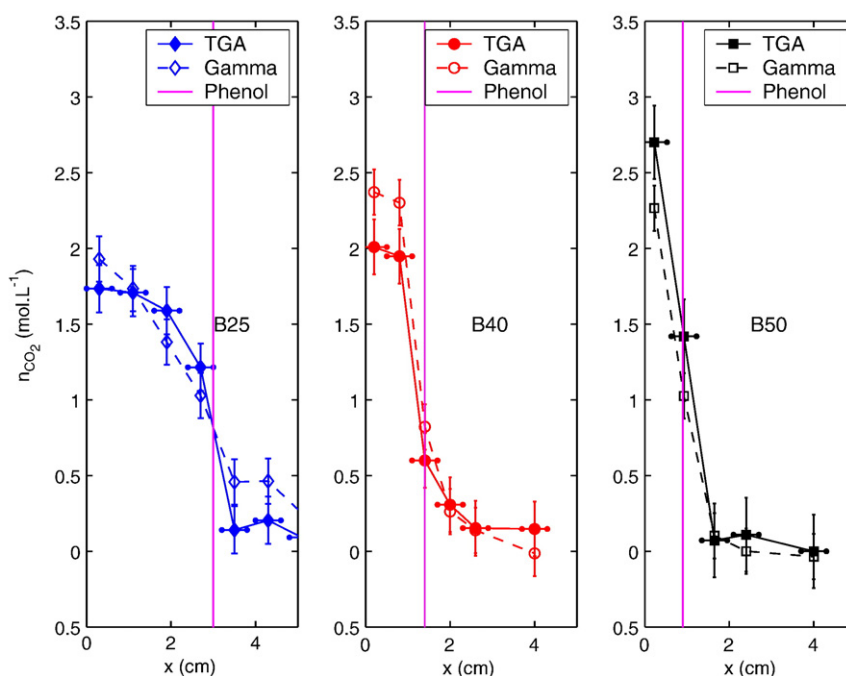

Fig. 7. CO_2 content profiles determined by TGA and gammadensitometry after a 14-day carbonation test of the concrete specimens.
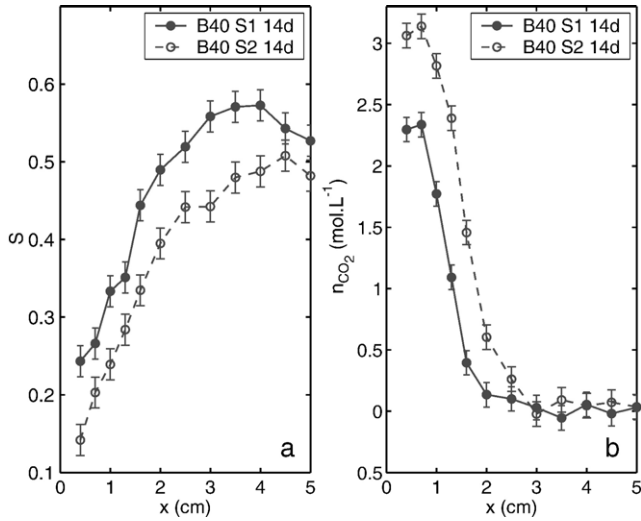
Fig. 8. Influence of the initial moisture state on the carbonation profile measured by gammadensitometry on the concrete B40 after 14 days of accelerated carbonation.

free for the diffusion of CO_2 through the porous network. Furthermore, the maximum level of carbonation near the surface is higher after the pre-treatment S2. Finally, it should be noticed that the carbonation profiles appear broader when the saturation degree is small after the pre-treatment.

Nonetheless, it is useful to recall that carbonation requires a certain amount of water since CO_2 and $Ca(OH)_2$ must dissolve, and ions have to enter in contact. This may explain the form of the gammadensimetric carbonation profile after a 3-day carbonation test of the B50 concrete specimen which is pre-dried according to pre-treatment S2 (see Fig. 9). Actually, the chemical reactions drastically slow down, and the progression of carbonation is reduced close to the surface exposed to the atmosphere where the concrete is very dry as compared to 1–2 cm deeper, where the water content is higher. After 7 days of accelerated exposure, the build-up of water due to carbonation of $Ca(OH)_2$ is likely to justify that the CO_2 dissolution kinetics are restored, and that the carbonation profile has a more usual shape.

4. Discussion of the effects of the chemical kinetics with an analytical model of carbonation

To identify the influence of the chemical kinetics on the carbonation progression, a model was developed. The following assumptions are made to obtain analytical results:

– The microstructural transformations and changes in water content induced by carbonation (in porosity and build-up of water), the C–S–H carbonation, the transport of ions and moisture are not taken into account.
– The CO_2 concentration in the atmosphere is supposed to be steady in time.
– Initially, porosity, liquid water saturation degree and $Ca(OH)_2$ content are uniformly distributed in the specimen.

4.1. Mathematical model for CO_2-diffusion and carbonation

A 1D diffusion-reaction problem is considered in the semi-infinite half space $x \geq 0$. n_i denotes the molar content of constituent i per unit volume of porous material. $[CO_2]$ is the CO_2 concentration in the gaseous phase. The CO_2-concentration in the aqueous phase is c_l. The mass conservation for the carbon element C can be written:

$$\frac{\partial n_C}{\partial t} = -\frac{\partial w_C}{\partial x} \tag{2}$$

where w_C denotes the molar flux of C. n_C is the molar content of C which is written:

$$n_C = \phi S[CO_2] + \phi(1-S)c_l + n_{CaCO_3} \tag{3}$$

where ϕ is the porosity and S is the liquid water saturation degree.

Given that the CO_2-diffusion coefficient in the gaseous phase is 10^4 times greater than the diffusion coefficient of the derived species in the liquid phase (H_2CO_3, HCO_3^- and CO_3^{2-}), it is assumed that the element carbon, C, is solely transported within the gaseous phase by means of diffusion, which gives $w_C \approx w_{CO_2}$.

The mass balance Eq. (2) has to be completed by the transport law of CO_2 through the porous medium. The basic relation for gas transport is Fick's law, which states that the driving force of the CO_2 transport is the concentration gradient. Formulated here in terms of the molar concentration gradient, Fick's law takes the form:

$$w_{CO_2} = -D_{CO_2}\frac{\partial[CO_2]}{\partial x} \ (\approx w_C) \tag{4}$$

where D_{CO_2} is a macroscopic diffusion coefficient for the average diffusive flow, which is expressed as the product of the diffusion coefficient D_{g0} of CO_2 outside the porous medium, by a factor, which is a function of both porosity ϕ and saturation level S of the material.
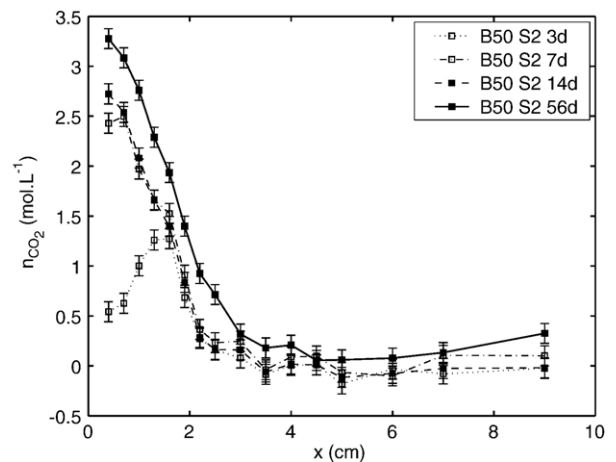

Fig. 9. CO_2 content profiles measured by gammadensitometry on a concrete B50 specimen at different stages of accelerated carbonation (3, 7, 14 and 56 days).

Experimental data (detailed in [36]) of the effective diffusion coefficient D_{CO_2} as a function of ϕ and S were fitted [37,38] using the following expression proposed by Millington [39]:

$$D_{CO_2} = \phi^a (1 - S)^b D_{g0} \tag{5}$$

with $a=2.74$ and $b=4.20$.

Within the framework of a simplified approach, the $CaCO_3$ growth rate is given by the rate Γ of the reaction represented by Eq. (1). Γ is assumed to have the following form:

$$\Gamma = \frac{\phi S}{\tau}(c_l - c_l^{eq}) \left(= \frac{\partial n_{CaCO_3}}{\partial t} = -\frac{\partial n_{Ca(OH)_2}}{\partial t} \right) \tag{6}$$

where τ is a characteristic time, which scales the rate at which the chemical reaction occurs and c_l^{eq} is the CO_2 concentration in solution at equilibrium. c_l^{eq} remains very low in comparison with common c_l values, and thus can be neglected [37,38].

A linear equilibrium law between CO_2 in the gaseous phase and CO_2 in the aqueous phase is assumed: $c_l = k[CO_2]$. By including these simplifications, the following reaction rate Γ can be written:

$$\Gamma = \frac{\phi S k}{\tau}[CO_2] \tag{7}$$

Note that the carbonation rate stops ($\Gamma=0$) when the saturation level S vanishes. This feature reflects the well-known result, according to which, once the liquid phase disappears, carbonation becomes impossible. Moreover, as soon as the initial $Ca(OH)_2$ content has been entirely consumed (i.e. $n_{CaCO_3}=n^i{}_{Ca(OH)_2}$), the reaction rate is 0.

The boundary condition for $x=0$ reflects the permanent contact of the cementitious material with an atmosphere, at a fixed CO_2 concentration $[CO_2]=[CO_2]_0$. The initial conditions express the fact that the material is not degraded at $t=0$. Moreover, the specimen is assumed to be long enough to justify the hypothesis of a semi-infinite medium. Thus, the initial and boundary conditions are the following ones:

$$\begin{cases} [CO_2](\forall x{\geq}0, t=0) = 0 \text{ and } n_{CaCO_3}(\forall x{\geq}0, t=0) = 0 \\ [CO_2](x=0, \forall t{>}0) = [CO_2]_0 \end{cases} \tag{8}$$

4.2. Dimensionless formulation

The following definitions are adopted:

$$u = \frac{[CO_2]}{[CO_2]_0}$$
$$v = 1 - \frac{n_{Ca(OH)_2}}{n^i_{Ca(OH)_2}} = \frac{n_{CaCO_3}}{n^i_{Ca(OH)_2}}$$
$$D = \frac{D_{CO_2}}{\phi(1 - S + kS)}$$
$$\varepsilon = \frac{[CO_2]_0 \phi(1 - S + kS)}{n^i_{Ca(OH)_2}}$$
$$T = \frac{\tau(1 - S + kS)}{kS}$$

The invariant parameters of this initial-boundary-value problem may be identified through the linear transformation of the whole set of involved variables, functions and parameters. It is found that functions u and v depend only on parameter ε, and on two variables:

$$z = \frac{x}{\sqrt{DT}} \text{ and } \eta = \frac{\varepsilon t}{T} \tag{9}$$

As a result, the studied problem may be expressed in the following dimensionless form:

$$\text{(a) } \varepsilon\frac{\partial u}{\partial \eta} + \frac{\partial v}{\partial \eta} = \frac{\partial^2 u}{\partial z^2} \quad \text{(b) } \frac{\partial v}{\partial \eta} = \begin{cases} u \text{ if } v < 1 \\ 0 \text{ if } v = 1 \end{cases}$$

With the boundary and initial conditions : \tag{10}
$$u(z = 0, \forall \eta{>}0) = 1$$
$$u(\forall z{>}0, \eta = 0) = 0$$
$$v(\forall z{>}0, \eta = 0) = 0$$

4.3. Edge effect and existence of a carbonation front

Eq. (b) in the system (10) represents the kinetics of the carbonation reaction and reveals that $Ca(OH)_2$ is not instantaneously consumed at the edge of the material (in $z=0 \Leftrightarrow x=0$). Mention can be made herein of an edge effect. Actually, a specific time T_S is necessary for $Ca(OH)_2$ to be fully consumed in $z=0$, where the CO_2 concentration is fixed at $[CO_2]_0$. This time is determined from Eq. (b) of the system (10) written in $z=0$:

$$\frac{\partial v}{\partial \eta} = \begin{cases} 1 \text{ if } v < 1 \\ 0 \text{ if } v = 1 \end{cases} \tag{11}$$

The $CaCO_3$ molar content formed at the surface is therefore given by:

$$\forall \eta{\leq}1 : v(z = 0, \eta) = \eta \text{ and } \forall \eta{\geq}1 : v(z = 0, \eta) = 1 \tag{12}$$

The expression of T_S is deduced:

$$T_S = \frac{\tau}{\varepsilon} \tag{13}$$

Then, for $\eta=1$ (i.e. $t=T_S$), all $Ca(OH)_2$ is depleted on the specimen edge in $x=0$. For $\eta \leq 1$ (i.e. $t<T_S$), the surface is undergoing carbonation, and for $\eta \geq 1$ (i.e. $t \geq T_S$), a carbonation front progresses within the material, and separates an entirely carbonated upstream zone (where $v=1$) from a degraded downstream zone where some $Ca(OH)_2$ is still present. This carbonation front is localized in $z=Z_C(\eta \geq 1) \Leftrightarrow x=X_C(t \geq T_S)$.

In the case $\eta \leq 1$, an analytical solution to this problem has been published by Danckwerts [40]:

$$\forall \eta{\leq}1 : u(z,\eta) = \cosh(z) - \frac{1}{2}\left[e^{-z}\text{erf}\left(z\frac{\sqrt{\varepsilon}}{2\sqrt{\eta}} - \sqrt{\frac{\eta}{\varepsilon}}\right) + e^z \, \text{erf}\left(z\frac{\sqrt{\varepsilon}}{2\sqrt{\eta}} + \sqrt{\frac{\eta}{\varepsilon}}\right) \right] \tag{14}$$

where the "erf" function (i.e. error-named function) is given by:

$$\mathrm{erf}(A) = \frac{2}{\sqrt{\pi}} \int_0^A e^{-a^2}\,\mathrm{d}a$$

u is plotted in Fig. 10 for $\eta = 0.1\varepsilon$, $\eta = \varepsilon$ and $\eta = 1$.

The following equation for v may also be written:

$$\forall \eta \leq 1 : v(z,\eta) = \int_0^\eta u(z,a)\,\mathrm{d}a \qquad (15)$$

4.4. Resolution for a small value of parameter ε

The solution to system (10) can be established for a small value of parameter ε. From a physical standpoint, this situation corresponds with the case, where the initial content of potentially-carbonated $Ca(OH)_2$ is much higher than the CO_2 concentration available both in the gaseous phase and in aqueous solution. Generally, it proves to be the case of typical cementitious materials, even under accelerated carbonation, since $[CO_2]_0 = 0.02$ mol L^{-1} for a 50% CO_2–50% air gas mixture in the test chamber and $n^i_{Ca(OH)_2}{}^i \geq 1$ mol L^{-1} for usual cementitious materials composed of OPC.

For $z \ll 2\eta/\varepsilon$, Eq. (14) is simplified and thus u may be written as follows:

$$\forall z \ll 2\eta/\varepsilon \text{ and } \forall \eta < 1 : u(z,\eta) = \cosh(z) - \sinh(z)\mathrm{erf}\left(\sqrt{\eta/\varepsilon}\right) \qquad (16)$$

With the "erf" function moving close to 1 whenever its argument exceeds 2, i.e. $\eta > 4\varepsilon$, the following equation is obtained:

$$\forall z \ll 2\eta/\varepsilon \text{ and } \forall \eta \epsilon [4\varepsilon, 1] : u(z,\eta) = e^{-z} \qquad (17)$$

Using Eq. (15), it comes:

$$\forall z \ll 2\eta/\varepsilon \text{ and } \forall \eta \epsilon [4\varepsilon, 1] : v(z,\eta) = \eta e^{-z} \qquad (18)$$

Therefore, for $\varepsilon \ll 1$ and as long as all of $Ca(OH)_2$ has not been degraded in $z = 0$ (i.e. $\eta < 1$), u quickly stabilizes in the
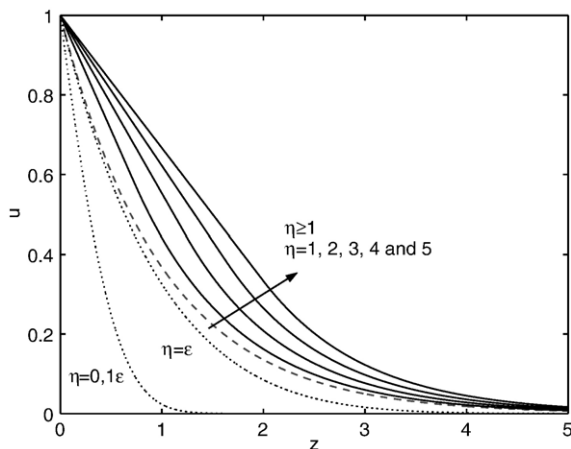

Fig. 10. Profiles of the function u vs. z for various values of η.

form of a decreasing exponential of variable z, independently of η (and thus of time t), as illustrated in Fig. 10.

For $\eta \geq 1$, the reaction front (in $z = Z_C$) can be localized at the last point from the surface where $v = 1$ (see Fig. 11). This reference point also corresponds to the z value for which the reaction rate reaches its maximum.

In the case $\eta \geq 1$ with $\varepsilon \to 0$, this diffusion–reaction problem has been investigated by Thiery et al. [37,38] and Mainguy [41]: the analytical expressions of functions Z_C, u and v are listed in Table 3; they are also depicted in Fig. 10 (for u) and Fig. 11 (for v and Z_C).

4.5. Infinitely rapid chemical reaction of carbonation (τ→0)

When the characteristic time τ tends to 0, the chemical reactions which are involved in the carbonation process are irreversible, and very rapid compared with the CO_2 diffusion: the chemical reactions are considered to take place at equilibrium. Thus, an essential characteristic feature is that a sharp boundary surface (the carbonation front) moves through the material as CO_2 diffusion proceeds, separating a region where all $Ca(OH)_2$ is depleted (for $z < Z_C \Leftrightarrow x < X_C$: $v = 1$) from an intact region ($z > Z_C \Leftrightarrow x > X_C$: $v = 0$). This means that, in front of the advancing boundary, the concentration of gaseous CO_2 is 0 and no chemical reaction has already occurred, while the reaction is complete behind it. This case corresponds to a diffusion–reaction process, in which diffusing molecules

Fig. 11. Profiles of v vs. z for various values of η. Depth of carbonation Z_C vs. η.

Table 3
Summary table of the analytical forms of solutions Z_C, u and v

$\forall \eta \in [4\varepsilon,1]$	$\forall \ll 2\eta/\varepsilon$	$u(z,\eta) = e^{-z}$
		$v(z,\eta) = \eta e^{-z}$
$\forall \eta \geq 1$		$Z_C(\eta) = \sqrt{2\eta - 1} - 1$
	$\forall z \leq Z_C(\eta)$	$u(z,\eta) = 1 - z/[1 + Z_C(\eta)]$
		$v(z,\eta) = 1$
	$\forall z \geq Z_C(\eta)$	$u(z,\eta) = e^{-[z - Z_C(\eta)]}/[1 + Z_C(\eta)]$
		$v(z,\eta) = e^{-[z - Z_C(\eta)]}$

(CO_2) are rapidly and permanently withdrawn by a limited number of reaction sites ($Ca(OH)_2$), and prevented from diffusing further.

Let us point out that for $\tau \to 0$, the variable η tends to infinity and hence an asymptotic approximation of Z_C (see Table 3) is:

$$Z_C(\eta) = \sqrt{2\eta} \qquad (19)$$

Thus, a more classical form for the carbonation depth is:

$$X_C(t) = \sqrt{\frac{2D_{CO_2}[CO_2]_0}{n^i_{Ca(OH)_2}}} \sqrt{t} \qquad (20)$$

The result proposed by Papadakis et al. [42] is consistent with Eq. (20). These authors directly reported that carbonation is controlled by the CO_2 diffusion, i.e. that the chemical reactions are all instantaneous.

4.6. Discussion about the "kinetic effects"

In Section 4, the analytical solutions to the initial-boundary-value problem of CO_2 diffusion, which is coupled with carbonation in a cementitious material has been exhibited. At this point, it is interesting to assess the characteristic time τ with a calibration. This step is carried out by using the results of accelerated carbonation tests, which have been obtained for the P45 cement paste. The average saturation degree S of the specimen has been determined from the experimental water-vapor desorption isotherm (available in [43]), and by making the assumption that the specimens have reached a moisture equilibrium with the carbonation chamber where RH=53%.

The simplified model developed here does not allow the incorporation of the $Ca(OH)_2$, which is present behind the carbonation front detected by the phenolphtalein-spray test, i.e. for $x<X_C$. A residual content (of about 0.6 mol L^{-1}) has been measured within this region (see Fig. 2): it constitutes a reserve of potentially non-carbonated hydrates or, at least, hydrates

Fig. 12. v profiles for the P45 cement paste after 14 and 28 days of accelerated exposure. Experimental and simulated profiles.

whose potential carbonation occurs too slowly on the time scale of the accelerated carbonation test. This residual content is thus subtracted from the $Ca(OH)_2$ content which is measured in the intact region at the core of the specimen (i.e. ≈ 5.6 mol L^{-1}). On the whole, we consider that $n^i_{Ca(OH)_2} \approx 1$ mol L^{-1}.

A length $\delta = \sqrt{DT}$ may be defined to characterize the carbonation progression on the experimental v-profile (see Fig. 12); it corresponds to the width of the carbonation front:

$$\delta = \sqrt{DT} = \sqrt{D_{CO_2} \frac{\tau}{k\phi S}} \qquad (21)$$

A graphical interpretation of the experimental profile after a 14-day accelerated carbonation test gives $\delta = 8 \cdot 10^{-3}$ m (see Fig. 12).

The carbonation depth X_C may be written as a function of both δ and T_S (see Eqs. (13) and (21), and the expression of Z_C in Table 3):

$$\forall t \geq T_S : X_C(t) = \delta \left(\sqrt{\frac{2t}{T_S} - 1} - 1 \right) \qquad (22)$$

With Eq. (22), the knowledge of δ and X_C after 14 days of accelerated exposure ($X_C \approx 1$ cm according to the phenolphthalein spray-test) makes it possible to identify T_S, i.e.: $T_S \approx 3.9 \cdot 10^5$ s (≈ 4 days and 14 h).

Another version of Eq. (13) is given by the following expression of the initiation time T_S as a function of the material physicochemical characteristics:

$$T_S = \frac{n^i_{Ca(OH)_2}}{[CO_2]_0} \left(\frac{\tau}{\phi Sk} \right) \qquad (23)$$

Eq. (23) makes it possible to compute $\tau/(\phi Sk)$ as equal to $1.6 \cdot 10^3$ s. By reinserting $\tau/(\phi Sk)$ into Eq. (21), the CO_2 diffusion coefficient may be evaluated at $4.0 \cdot 10^{-8}$ m^2 s^{-1}. This value is comparable to that obtained from the empirical "fitting" of a diffusion law (see Eq. (5)), i.e. $D_{CO_2} = 6.5 \cdot 10^{-8}$ m^2 s^{-1}.

In addition, knowing both ϕ and S, the term τ/k can be evaluated; it represents the chemical kinetics effects. A value of $\tau/k \approx 320$ s has been found.

Thanks to the calibration of τ/k from experimental results after a 14-day accelerated exposure, the theoretical v-profile can be calculated after 28 days of accelerated carbonation. This computation corroborates experimental data quite well (see Fig. 12).

Similarly, the carbonation depth X_C predicted by the model after 7 and 28 days of accelerated exposure is consistent with the phenolphthalein-derived depths (see Fig. 13). Furthermore, it is possible to identify in this figure the time T_S, necessary for carbonation to be sufficiently advanced at $x=0$ to make the pH-value drop below 9. It is found that $T_S \approx 4$ days, which is consistent with the calibration results. It should also be noted that in this same figure, X_C deviates significantly from the experimental data when it is simulated by assuming that the characteristic time τ tends to 0. This result indicates that it is thus
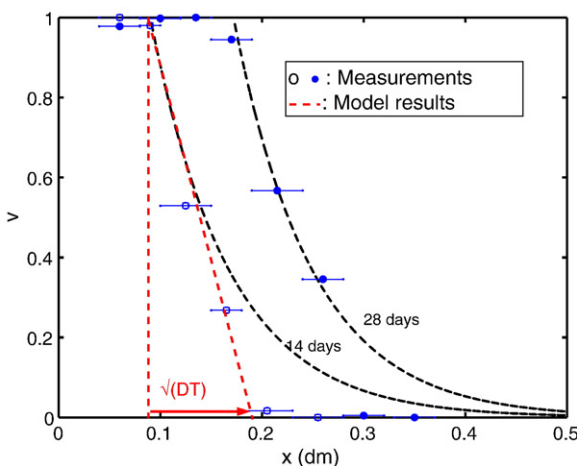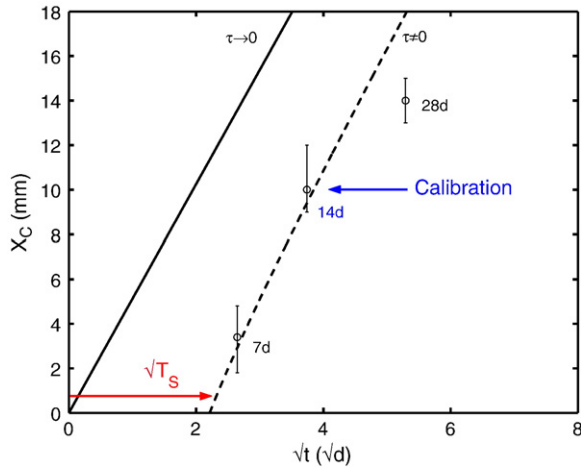
Fig. 13. Carbonation depth vs. time obtained both from experiments (phenolphtalein spray test) and from numerical simulations for the P45 cement paste.

legitimate to introduce this concept of chemical kinetic, characterised by a reaction time, in the modelling of the carbonation process.

In the light of this carbonation model, it is possible to identify and quantify the influence of the chemical reactions kinetics and of various physical parameters of transport (like the water saturation level S and the porosity ϕ) on the carbonation front shape. In this diffusion–reaction problem, two time scales can be distinguished in the system (10):

$$\tau_R = \tau \frac{1 - S + kS}{kS} \qquad (24)$$

$$\tau_D = \frac{L^2 \phi}{D_{CO_2}(\phi, S)} [1 - S + kS] \qquad (25)$$

The CO_2-diffusion coefficient D_{CO_2} is given by Eq. (5). τ_R is characteristic for the chemical reaction and τ_D for the CO_2 diffusion. L is the structural dimension which characterizes the macroscopic volume of the tested specimen (≈ 10 cm for our specimens). According to Eq. (21), the carbonation front width δ is given by:

$$\delta = L \sqrt{\frac{\tau_R}{\tau_D}} \qquad (26)$$

δ is governed by the ratio τ_R / τ_D. It can be admitted that $\tau_R < \tau_D$ in the case of our carbonation–diffusion problem. Nevertheless, when these two times differ significantly from each other ($\tau_R \ll \tau_D$), δ tends to 0 and the carbonation front is rather sharp. On the other hand, if τ_R and τ_D are of similar magnitude the carbonation front is more gradual. Thus, the more porous the concrete is, the broader the carbonation front is, since τ_D is decreased (see Eq. (25)). The experimental gammametric results, which are shown in Fig. 7 for the concrete mixtures studied, indicate that the carbonation profile is broader for a low-grade concrete like B25 (with a high porosity > 15%) than for a normal strength-concrete B50 (with a weaker porosity). In the same way, the dryer the concrete is, the smaller τ_D is (see

Eq. (25)) and the more δ is increased, as it has been illustrated in Fig. 8.

5. Concluding remarks

Gammadensitometry and thermogravimetric analysis (TGA) were used to characterize the partially carbonation region which is not detectable by the classical phenolphtalein spray test.

Gamma-ray measurements illustrate carbonation profiles of various concrete mixtures which were carbonated under accelerated carbonation. This method makes it possible to follow the global fixation of CO_2 in the concrete, and shows that the carbonation front is not sharp.

C–S–H and $Ca(OH)_2$ carbonation profiles were determined by TGA, completed by a chemical analysis, for the concrete mixtures and a cement paste. The shape of the carbonation front for these two hydrates is not sharp. Furthermore, TGA profiles indicate that the $Ca(OH)_2$ carbonation is initially more rapid than that of the C–S–H gel, but this situation soon reverses because of the formation of a layer of calcium carbonate $CaCO_3$ microcrystals at the $Ca(OH)_2$ crystals surface. In addition, a residue of $Ca(OH)_2$ does not carbonate and cannot maintain a high pH-value in the pore solution. These observations are consistent with a rate-determining stage controlled by the reduction of accessibility of $Ca(OH)_2$ crystals which are coated with $CaCO_3$ during the carbonation process. Eventually, the TGA results indicate that CO_2 is chemically bound as $CaCO_3$ which precipitates in various forms, namely stable, metastable, and amorphous $CaCO_3$. It seems that the thermal stability of $CaCO_3$ produced is lower as the carbonation level is higher. It is also shown that the poorly crystallized and thermodynamically metastable forms of $CaCO_3$ correspond to the carbonation of C–S–H.

The model of carbonation presented yields analytical results that make it possible to identify the significance of the chemical kinetics within the carbonation process, and to quantify a characteristic time for chemical reaction. In particular, it has been shown that the width of the carbonation front is directly linked to these kinetic effects, since it is governed by the ratio of two time scales, τ_R and τ_D, associated with the chemical reaction of carbonation and with the CO_2-diffusion. The width of carbonation front is broader when these two time scales are of similar magnitude, for instance when the reaction time is high (if the chemical reaction is not instantaneous), or when the CO_2 diffusion is facilitated (if the concrete is very porous and/or dry). In this approach, the global chemical reaction rate was used, assuming that all the chemical reactions were homogeneous. This may be considered as a macroscopic approach in terms of chemical kinetics. In reality, the effective carbonation mechanism cannot be considered as a homogeneous reaction (between reactants from the same phases). Dissolution of $Ca(OH)_2$ and precipitation of $CaCO_3$ are both heterogeneous reactions (between a liquid-phase and a solid-phase) whose kinetics depend on the surface area of $Ca(OH)_2$ and $CaCO_3$. Moreover, they also depend on the initial $Ca(OH)_2$ content within the material, which differs between a concrete or a cement paste: for

instance, the M25 concrete contains five times less Ca(OH)$_2$ than the P45 cement paste.

References

[1] V.A. Juvekar, M.M. Sharma, Absorption of CO$_2$ in a suspension of lime, Chem. Eng. Sci. 28 (1973) 825–837.

[2] S.E. Pihlajavaara, Some results of the effect of carbonation on the porosity and pore size distribution of cement paste, ACI Mater. Struct. 1 (6) (1968) 521–526.

[3] Z. Sauman, Carbonation of porous concrete and its main binding components, Cem. Concr. Res. 1 (1971) 645–662.

[4] P.A. Slegers, P.G. Rouxhet, Carbonation of the hydration products of tricalcium silicate, Cem. Concr. Res. 6 (1976) 381–388.

[5] K. Suzuki, T. Nishikawa, S. Ito, Formation and carbonation of C–S–H in water, Cem. Concr. Res. 15 (1985) 213–224.

[6] K. Kobayashi, K. Suzuki, Y. Uno, Carbonation of concrete structures and decomposition of C–S–H, Cem. Concr. Res. 24 (1994) 55–61.

[7] T. Nishikawa, K. Suzuki, S. Ito, Decomposition of synthesized ettringite by carbonation, Cem. Concr. Res. 22 (1992) 6–14.

[8] C. Xiantuo, Z. Ruizhen, Kinetic study of ettringite carbonation reaction, Cem. Concr. Res. 24 (7) (1994) 1383–1389.

[9] Q. Zhou, F.P. Glasser, Kinetics and mechanism of the carbonation of ettringite, Adv. Cem. Res 12 (3) (2000) 131–136.

[10] Y.F. Houst, F.H. Wittmann, Influence of porosity and water content on the diffusivity of CO$_2$ and O$_2$ through hydrated cement paste, Cem. Concr. Res. 24 (6) (1994) 1165–1176.

[11] V.T. Ngala, C.L. Page, Effect of carbonation on pore structure and diffusional properties of hydrated cement pastes, Cem. Concr. Res. 27 (7) (1997) 995–1007.

[12] M. Thiery, G. Villain, G. Platret, Effect of carbonation on density, microstructure and liquid water saturation of concrete, in: D.A. Lange, K.L. Scrivener, J. Marchand (Eds.), Advances in Cement and Concrete IX, Engineering Conferences International, Copper Mountain, Colorado, USA, 2003, pp. 481–490.

[13] L. De Ceuklaire, D. Van Nieuwenburg, Accelerated carbonation of a blast furnace cement concrete, Cem. Concr. Res. 23 (1993) 442–452.

[14] H. Wierig, Long time studies on the carbonation of concrete under normal outdoor exposure, RILEM Seminar, Hanover, Germany, 1984, pp. 239–249.

[15] T. Saeki, H. Ogha, S. Nagataki, Mechanism of carbonation and prediction of carbonation process of concrete, Concrete Library of JSCE, v ol. 12 (414), 1991, pp. 23–36.

[16] A.A. Rahman, F.P. Glasser, Comparative studies of the carbonation of hydrated cements, Adv. Cem. Res 2 (6) (1989) 49–54.

[17] Y.F. Houst, F.H. Wittmann, Depth profiles of carbonates formed during natural carbonation, Cem. Concr. Res. 32 (12) (2002) 1923–1930.

[18] G. Villain, M. Thiery, G. Platret, Measurement methods of carbonation profiles in concrete: thermogravimetry, chemical analysis and gamma-densimetry, Cem. Concr. Res. (in press).

[19] Y. Lo, H.M. Lee, Curing effects on carbonation of concrete using a phenolphthalein indicator and Fourier-transform infrared spectroscopy, Build. Environ. 37 (2002) 507–514.

[20] M. Hamada, Neutralization (carbonation) of concrete and corrosion of reinforcing steel, in: The Cement Association of Japan (Eds.), 5th International Symposium on Cement Chemistry, Tokyo, Japan, 1968, pp. 343–369.

[21] G. Villain, M. Thiery, Gammadensimetry: a method to determine drying and carbonation profiles in concrete, NDT&E International, vol. 39(4), 2005, pp. 328–337.

[22] L.J. Parrott, D.C. Killoh, Carbonation in a 36 year old in situ concrete, Cem. Concr. Res. 19 (1989) 649–656.

[23] G.W. Groves, A. Brough, I.G. Richardson, C.M. Dobson, Progressive changes in the structures of hardened C$_3$S cement pastes due to carbonation, J. Am. Ceram. Soc. 74 (11) (1991) 2891–2896.

[24] G.W. Groves, D.I. Rodway, I.G. Richardson, The carbonation of hardened cement pastes, Adv. Cem. Res 3 (11) (1990) 49–54.

[25] A.M. Dunster, An investigation of the carbonation of cement paste using trimethylsilylation, Adv. Cem. Res 2 (7) (1989) 99–106.

[26] D.R. Glasson, Reactivity of lime and related oxides, part VI: crystal changes in carbonated lime at different temperatures, J. Appl. Chem. 11 (1961) 28–34.

[27] W.F. Cole, B. Kroone, Carbon dioxide in hydrated Portland cement, ACI J. 31 (12) (1960) 1275–1295.

[28] G. Villain, G. Platret, Two experimental methods to determine carbonation profiles in concrete, ACI Mater. J. 103 (4) (2006) 265–271.

[29] R. Kondo, M. Daimon, T. Akiba, Mechanisms and kinetics on carbonation of hardened cement, 5th International Symposium on Cement Chemistry, Tokyo, Japan, vol. III, 1969, pp. 402–409.

[30] T. Ogino, T. Suzuki, K. Sawada, The formation and transformation mechanism of calcium carbonate in water, Geochim. Cosmochim. Acta 51 (1987) 2757–2767.

[31] L. Brecevic, A.E. Nielsen, Solubility of amorphous calcium carbonate, J. Cryst. Growth 98 (1959) 504–510.

[32] E. Usdowski, Reactions and equilibria in the systems H$_2$O and CaCO$_3$–CO$_2$–H$_2$O, N. Jb. Miner. Abh. 144 (2) (1982) 148–171.

[33] L.N. Plummer, E. Busenberg, The solubilities of calcite, aragonite and vaterite in CO$_2$–H$_2$O solution between 0 and 90 °C, and an evaluation of the aqueous model for the system CaCO$_3$–CO$_2$–H$_2$O, Geochim. Cosmochim. Acta 46 (1982) 1011–1040.

[34] C.M. Hunt, L.A. Tomes, Reaction of blended Portland cement paste with carbon dioxide, J. Res. Natl. Bur. Stand. 66 (A) (1962) 473–481.

[35] T. Chaussadent, Etat des lieux et réflexions sur la carbonatation du béton armé, Etudes et Recherches des Laboratoires des Ponts et Chaussées, Laboratoire Central des Ponts et Chaussées, Paris, 1999.

[36] V.G. Papadakis, C.G. Vayenas, M.N. Fardis, Physical and chemical characteristics affecting the durability of concrete, ACI Mater. J. 88 (2) (1991) 186–196.

[37] M. Thiery, P. Dangla, G. Villain, G. Platret, E. Massieu, M. Druon, V. Baroghel-Bouny, Modelling the atmospheric carbonation of cementitious materials, Bul. Labo. des Ponts et Chaussées, vol. 252–253, 2004, pp. 153–187, http://www.lcpc.fr/en/sources/index.dml.

[38] M. Thiery, Modélisation de la carbonatation atmosphérique des matériaux cimentaires — Prise en compte des effets cinétiques et des évolutions microstructurales et hydriques. PhD Thesis, Ecole Nationale des Ponts et Chaussées, Paris, 2005.

[39] R.J. Millington, Gas diffusion in porous media, Science 130 (1959) 100–102.

[40] P.V. Danckwerts, Absorption by simultaneous diffusion and chemical reaction, Trans. Faraday Soc. 46 (1950) 300–304.

[41] M. Mainguy, Modèles de diffusion non-linéaires en milieux poreux. Applications à la dissolution et au séchage des matériaux cimentaires. PhD Thesis, Ecole Nationale des Ponts et Chaussées, Paris, 1999.

[42] V.G. Papadakis, C.G. Vayenas, M.N. Fardis, Fundamental modeling and experimental investigation of concrete carbonation, ACI Mater. J. 88 (4) (1991) 363–373.

[43] V. Baroghel-Bouny, M. Mainguy, T. Lassabatère, O. Coussy, Characterization and identification of equilibrium and transfer moisture properties for ordinary and high-performance cementitious materials, Cem. Concr. Res. 29 (1999) 1225–1238.